THE ASTRONOMICAL JOURNAL VOLUME 111, NUMBER 3 MARCH 1996

NGC 6210: AN OBSERVATIONAL CASE STUDY OF A JET EMITTING SOURCE

J. P. PHILLIPS

Instituto Nacional de Astrofisica, Optica y Electronica, A. Postal 51 y 216, Codigo Postal 72000, Puebla, Mexico
Electronic mail: jpp@tonali.inaoep.mx

L. CUESTA

Instituto de Astrofisica de Canarias, La Laguna, Tenerife, Spain
Electronic mail: lcc@ll.iac.es

Received 1995 August 21; revised 1995 December 13

ABSTRACT

We have acquired low- and intermediate-resolution spectroscopy at 11 positions across the nucleus of NGC 6210. As a consequence, we are able to map the variation of velocity, temperature, line excitation, and density over the projected core and halo of this source. Temperatures reach a peak value $T_e \cong 1.1\times10^4$ K close to the nucleus, and thereafter decline by ~24% towards the periphery of the core, some 7.5 arcsec from the central star. By contrast, density peaks towards the north, achieving maximal values $n_e \cong 6.1\times10^3$ cm^{-3}, and subsequently falls by ~72% towards the southern limits of the region; a distribution which is reminiscent of (and presumably causally related to) the observed radio structure. Line excitation is highly variable, with low-excitation lines particularly enhanced to the NW, along arms extending NW and (to a lesser degree) SE into the halo, and close to a bright condensation located some ~17 arcsec outside of the primary shell. These low-excitation extensions, and the associated NW condensation, appear also to be the location of a significant kinematic disturbance; a feature which is narrowly focused, and possesses characteristics reminiscent of a highly collimated jet. It is apparent, in brief, that the nucleus of NGC 6210 is ejecting material along two, and possibly four opposing directions, with curvature of this outflow indicating possible rotation of the collimating source. The kinematics of the halo appear to be similarly disturbed, with evidence for at least three circularly symmetric, low-amplitude ripples extending through the exterior velocity field. Halo linewidths appear also to be appreciable, of order 50 km s^{-1}, although the precise origin of this broadening remains far from clear. Finally, and in keeping with the maps of density and line excitation, it is clear that the velocity structure of the core is by no means straightforward. Detailed consideration of our results suggests, however, that we may be observing a partially disrupted shell, of type recently proposed in the cases of NGC 6905 and NGC 7026. In particular, the kinematic trends for locations close to P.A.=335° are reminiscent of spheroidal expanding shells—although with notable disparities which may suggest some elongation or fragmentation of the outflow. Alternatively, orthogonal axes reveal strongly variable, and more-or-less parallel velocity trends between front and rear shells, resulting in positive velocities to the west, and corresponding negative velocities to the east. Such a tendency can be reasonably modeled in terms of a pseudocylindrical outflow structure, provided we assume appreciable ionization stratification, substantial radial velocity gradients, and that the exterior has appreciable nonradial asymmetries arising from localized fragmentation. © *1996 American Astronomical Society.*

1. INTRODUCTION

NGC 6210 is an unusual compact source with core dimensions $\Delta\alpha\times\Delta\delta \approx 22\times18$ arcsec^2. Images in Hα reveal a diffuse, somewhat squarish morphology, although corresponding [N II] and He II photographs suggest a concentration of emission towards the north (Balick 1987; Icke *et al.* 1989); a tendency which is also favored by the 6 cm radio continuum (Terzian 1987). Estimates of central star temperature have varied considerably over the years (cf. Kaler 1986; Aller & Epps 1975; Aller & Czyzak 1989), with perhaps the most reliable recent values indicating $T_{\rm eff}\sim6.8\times10^4$ K (Preite-Martinez 1993), while mean densities are moderate and of order $\sim7\times10^3$ cm^{-3} (Aller & Czyzak 1989; Aller & Epps 1975; Stanghellini & Kaler 1989). Estimates of central star wind parameters also indicate outflow velocities of 2180 km s^{-1}, and mass-loss rates $dM/dt \cong 2.2\times10^{-9}$ $\mathcal{M}_\odot$ yr^{-1} (Perinotto 1993), similar to the values found in other moderate luminosity *PN* (Cerruti-Sola & Perinotto 1989).

There have been no detailed studies of this nebula before, although the kinematics has recently been briefly considered by Icke *et al.* (1989). As a consequence, it is clear that the outflow structure is complex, with some evidence for a dichotomy of velocities over the core; eastern sections of the nebula appear to possess large negative velocities, western sections corresponding positive velocities. Long exposure imaging of the source also reveals the presence of a broadly circular halo with diameter ~65 arcsec, containing two pairs of arm-like extensions on opposing sides of the nucleus (Balick *et al.* 1992; Duncan 1937).

 0004-6256/96/111(3)/1227/14/$6.00

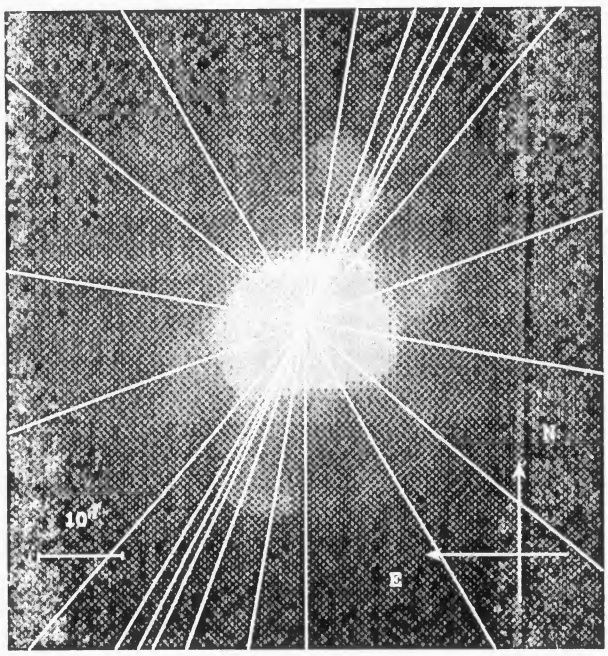

FIG. 1. Superimposition of the high-resolution slit positions upon an Hα +[N II] image of NGC 6210 adapted from Balick *et al.* (1992). Note the extended halo containing two sets of symmetrically disposed arms; the slit locations are concentrated about the brightest of these components. A bright condensation/ansa noted in our spectra, having P.A.=333° and relative position 17 arcsec, appears to coincide with an emission enhancement within the most northerly of these features.

In the present paper, we present the first detailed kinematic and structural analysis of the source using low- and intermediate-resolution spectroscopy. As a result, we will establish the detailed temperature and density variation over the shell, evaluate trends in line excitation and velocity, and note the presence of a jet-like feature associated with enhanced low-excitation halo emission.

2. OBSERVATIONS

Observations of NGC 6210 were acquired during 1991 June, using the $f/15$ Isaac Newton Telescope at the Observatorio del Roque de Los Muchachos, La Palma (ORM). An Intermediate Dispersion Spectrograph, 500 mm camera, and CCD detection element, together with gratings corresponding to a dispersion of 10.5 Å mm^{-1} ($\equiv$0.22 Å pixel^{-1}; H1800V) and 66.1 Å mm^{-1} ($\equiv$1.45 Å pixel^{-1}; R300V) were employed to obtain low-resolution spectra in the blue (4240–5070 Å) and red (6170–7010 Å), and higher-resolution observations in the red, centered upon Hα. The slit length was in all cases 180″, and the effective spatial resolution 0.33 arcsec pixel^{-1}. The low spectral resolution observations were acquired at position angles 20°, 50°, 80°, 110°, 333°, and 350° through the nucleus, while those at high-resolution spectra were obtained at 0°, 30°, 50°, 80°, 110°, 140°, 330°, 333°, 335°, 340°, and 350°. The locations of the high-resolution slit positions are indicated in Fig. 1, superimposed upon an Hα+[N II] image of the nebula due to Balick *et al.* (1992).

Seeing was more-or-less constant, of order 0.9–1.2 arcsec, while exposure periods varied from 400 s at high resolution, to 500 s at low resolution. Wavelength calibration was accurate to 0.09 Å at high resolution, and 0.5 Å at low resolution, while flux calibration was undertaken using the standard stars Feigle 15 and Kopff 27, together with an extinction curve appropriate to the ORM.

The data are summarized in a series of Figs. 1–16, where we include information on the emission structure and line ratio trends (Figs. 2–6), variation in line velocities and widths (Figs. 8–14), and derivative parameters such as temperature (Fig. 16) and density (Fig. 15). Finally, a listing of observed (I) and extinction corrected (I_c) line intensities is provided in Table 1, wherein we detail values appropriate for various sectors of the nebula. The assumed mean extinction $c=0.047$ is based upon present observations (see Sec. *4.1*).

3. RESULTS

3.1 The Excitation and Emission Structure of NGC 6210

Spatial emission profiles through the nucleus of NGC 6210 are illustrated in Fig. 2, where we indicate the variation arising for both low- and high-excitation transitions along a P.A. of 333°. Although the behavior of these profiles is dependent upon the particular angular traverse selected, the general trends are characteristic for all P.A.'s.

There appears to be an appreciable variation in source structure as between the various transitions. Thus, low-excitation lines such as [O I] λ6300, [S II] λλ 6717+6731 and [N II] λ6584 peak at somewhat negative axial displacements (that is, towards the north and west of the central star); Hβ, [O III], and He I display a broad and convex profile centered about the nucleus; while [O III], [N III], He II, and [Ar IV] appear significantly narrower, and possessed of Gaussian emission profiles. At the very least, it is clear that we are dealing with a source characterized by an unusual and complex pattern of excitation.

It is also possible to use our low resolution spectroscopy to illustrate the projected two-dimensional variation in line ratios, as in Fig. 3, whence we see clear evidence for a ring of enhanced [O III]/Hβ emission about the nucleus; a northwesterly increase in relative low-excitation strengths within the core (apparently dual peaked), and an arc of low-excitation emission located at the halo condensation (in the case of [O I]), and also extending between the condensation and inner shell (in the cases of [N II] and [S II]). A word of caution is appropriate at this point. The interpolative mapping routine results in some azimuthal smearing, to a degree which depends upon the rate of angular sampling. Such effects will, in general, be more pronounced at larger radii, such that the observed angular extent of the [O I] condensation is considerably in excess of the intrinsic dimensions of this feature. Inspection of the original data reveals that emission is present for P.A.=333° alone; the intrinsic size (if presumed similar to that of [N II] emission, sampled in the more extensive higher-resolution data set) would be $5°<\theta_a<20°$.

Finally, the complexity in source excitation may also be usefully illustrated through the ratio of [N II] and Hα IDS

TABLE 1. Relative line strengths in NGC 6210.

λ	IDENT	NUCLEUS[1]		ANSA[2]		JET[3]		HALO[4]	
		I_0	I_c	I_0	I_c	I_0	I_c	I_0	I_c
4340	HI	44.9	45.7	35.7	36.3	-	-	-	-
4363	[OIII]	13.4	13.6	-	-	-	-	-	-
4387	He I	0.7	0.7	-	-	-	-	-	-
4471	He I	4.9	4.9	-	-	-	-	-	-
4364	[N III]	1.4	1.4	-	-	-	-	-	-
4649	[C III]	0.5	0.5	-	-	-	-	-	-
4686	He II	2.7	2.8	-	-	-	-	-	-
4711	[Ar IV]	2.1	2.1	-	-	-	-	-	-
4740	[Ar IV]	2.1	2.1	-	-	-	-	-	-
4861	HI	100.0	100.0	100.0	100.0	100.0	100.0	100.0	100.0
4922	He I	1.7	1.7	-	-	-	-	-	-
4931	[OIII]	0.1	0.1	-	-	-	-	-	-
4959	[OIII]	376.1	375.0	326.8	325.9	361.9	360.9	414.3	413.2
5007	[OIII]	850.4	846.8	983.5	979.4	1212.1	1207.0	1310.7	1305.1
5048	[He II]	0.1	0.1	-	-	-	-	-	-
6300	[OI]	1.7	1.6	4.6	4.4	-	-	-	-
6312	[S III]	3.1	3.1	2.9	2.8	-	-	-	-
6348	[Si II]	0.2	0.2	-	-	-	-	-	-
6364	[OI]	0.7	0.6	1.4	1.3	-	-	-	-
6500	[Ar II]	0.1	0.1	-	-	-	-	-	-
6548	[NII]	6.7	6.5	39.0	37.6	26.7	25.8	-	-
6563	HI	299.0	288.7	280.7	271.0	283.3	273.6	344.8	333.0
6584	[NII]	23.5	22.6	97.9	94.5	69.6	67.1	8.7	8.4
6678	He I	4.4	4.2	3.6	3.5	-	-	-	-
6717	[S II]	1.8	1.7	6.9	6.6	-	-	-	-
6731	[S II]	5.5	5.3	16.3	15.8	-	-	-	-

Notes: (1) Line strengths are for the six low resolution spectra combined integrated over the spatial range -6.5 arcsec ≤ RP ≤ 6.5 arcsec; (2) Line strengths for -18.5 arcsec ≤ RP ≤ -15.5 arcsec along PA = 333°; (3) Line strengths for -14.2 arcsec ≤ RP ≤ -10.0 arcsec along PA = 333°; (4) Line strengths for combined halo spectra having PA = 20°, 50°, 80°, 119°, and 350°.

spectra (Fig. 4). This reveals an appreciable variation in intensities with respect to both radius and velocity; differing levels of excitation appear to occur along the same line of sight, and the observed spatial variation in this ratio (cf. in Fig. 3) must therefore simplify what is in reality a much more complex structure.

3.2 Emission Properties of the Halo

In addition to the more general properties cited above, we wish to emphasize several more particular characteristics of the emission structure confined to the halo region alone. First, and as noted in a sampling of the IDS [N II] and H I λ6563 spectra illustrated in Fig. 5, the emission structure of the halo is highly variable, both in structure and intensity. The apparent absence of extended [N II] emission arises, primarily, because of the limited sensitivity of individual spectra. Nevertheless, [N II] λ6584 Å intensities for halo regimes exterior to the nebular arms are indeed low, and of order ~8.7 (for $H\beta=100$), a value which may be compared to 23.5 for the nebular core, and ~98 for the halo condensation (see Table 1).

The Hα emission trends reveal extremely weak halo extensions along a P.A. of 50°, strengthening significantly along a P.A. of 350°, where there is weak evidence for a southerly halo maximum, and otherwise broadly symmetric bars of emission. Finally, results along position angle 333° pick up the exterior condensation noted in the photograph of Balick *et al.* (1992), a feature which is also strong in [N II]. A perusal of this image (Fig. 1) suggests that the condensation is located within an arm-like feature, an overall emission enhancement which appears also to have a counterpart to the SE, and is responsible for the symmetric appearance of the P.A.=350° line profile. A somewhat weaker symmetric structure is located along P.A.=105°. We shall later find that these arms of emission appear also to be associated with a kinematic disturbance. Note, by the way, the much clearer splitting of the core emission lines in [N II] as compared to Hα

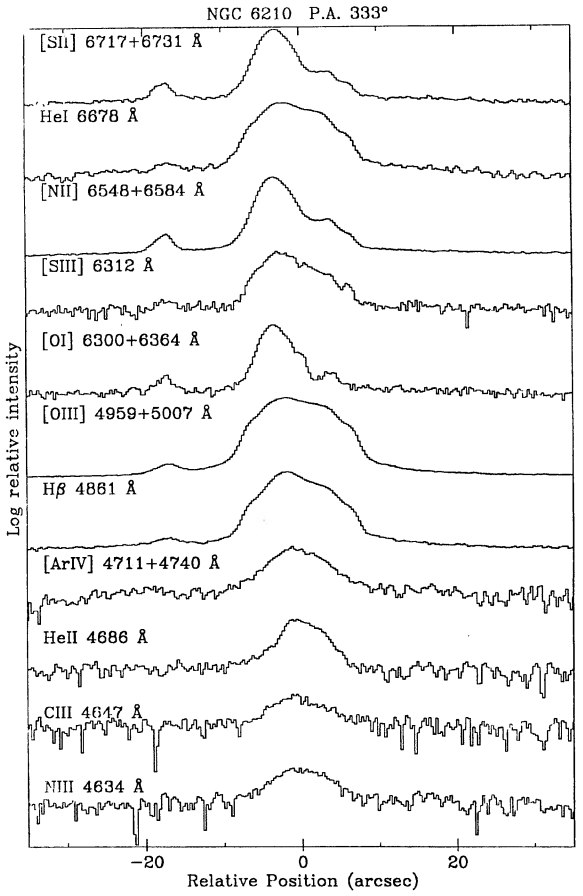

FIG. 2. Variation of line emission through the nucleus of NGC 6210 for position angle 333°. Notice the extreme variability displayed between lines of differing excitation, resulting in corresponding changes in apparent source FWHM.

(the Hα core lines are saturated in this representation, but in fact also possess a lower relief dual velocity structure). It is also possible with IDS spectra to delineate an enhancement close to λ=6560 Å, corresponding to the He II 4^2F-6^2G transition, although this is not included in the low-resolution line listings provided in Table 1.

The Hα emission structure of the halo is further illustrated in Fig. 6, where we show profiles corresponding to three differing slices through the nucleus. The intensity distributions differ appreciably for each case, with evidence for a rapid fading away in intensity for P.A.'s close to 80° and, as noted above, strong localized emission along a P.A. of 333° (corresponding to the halo condensation), together with a very much more symmetric and sharply defined structure, where P.A.=350°. Profiles along other P.A.'s possess intermediate structural characteristics.

3.3 Kinematic Structure of the Halo

The kinematic structure of the halo appears to be extremely complex, with large variations in the velocity pattern occurring for quite small changes in position angle. Some indication of these trends may be seen in Fig. 7, where we illustrate the variation of Hα and [N II] line centroid velocities as a function of axial displacement (both here and elsewhere, the variations are with respect to the median shell velocity).

Several features are apparent in this latter figure, as well as for the corresponding velocity maps illustrated in Figs. 9 and 10. In the first place, it is clear that [N II] line strengths are not very considerable within the halo, and our sampling of this transition is therefore relatively restricted. Where [N II] line velocities are accessible, however, it is clear that they are not greatly different from the corresponding Hα values; there is little evidence for the types of stratification effect one might anticipate for an extended halo having appreciable velocity gradients.

A second feature is the relative constancy of halo velocities over a broad sweep of position angles 0°–140°/180°–320°; the most distinctive changes in halo kinematics appear to be restricted to an extremely narrow range of P.A.'s centered upon P.A.=333° (that is, the axis containing the arm-like extensions, and exterior condensation noted in Sec. *3.1*). In particular, the largest velocity deviations, having maximum amplitude 21 km s^{-1} are associated with an extremely narrow emission regime located in the range 330°<P.A. <335°; a 5° span which is in turn enveloped by a region of lower amplitude disturbance of width $20°<\theta<40°$. It appears that we are observing a restricted and highly distinctive kinematic disturbance which extends on both sides of the nucleus; is present at all radii; and is associated with a corresponding enhancement in low-excitation emission (Sec. *3.1*), features similar to those observed for astrophysical jets within other sources.

The variation in velocity for this latter regime is further illustrated in Fig. 8, where we have superimposed trends for both positive and negative axial displacements. As a consequence, it is apparent that the opposing arms have velocity peaks at similar distances from the nucleus, although velocity gradients for positive relative positions with respect to the nucleus (RPs) are steeper at lower radial displacements, and by turns shallower at larger radial distances. A further feature of note is that apparent kinematic trends are almost certainly, in part, a function of the projected jet morphology. The downturn in velocities for radial displacements >20 arcsec, for instance, may reflect a genuine decline in flow velocities as distance from the nucleus increases. It is also apparent, however, that this is precisely the radius at which the arm-like features curl significantly away from the slit axis (Fig. 1), and it is unlikely, therefore, that we are continuing to measure the primary jet flow.

This radial kinematic feature is also evident in Figs. 9 and 10, where we note evidence for further lower amplitude disturbances in the halo velocity field. In particular, the velocity relief map shows the presence of ~3 circularly symmetric ripples having typical amplitude ~10 km s^{-1}. Although the numerical interpolation techniques used to construct this map can give rise to anomalous arcs over restricted angular ranges, the present trends appear to be consistent and real. Not only does the halo display properties reminiscent of jet activity, therefore, but it appears also to be prone to an underlying wave-like structure, centered upon the nucleus.

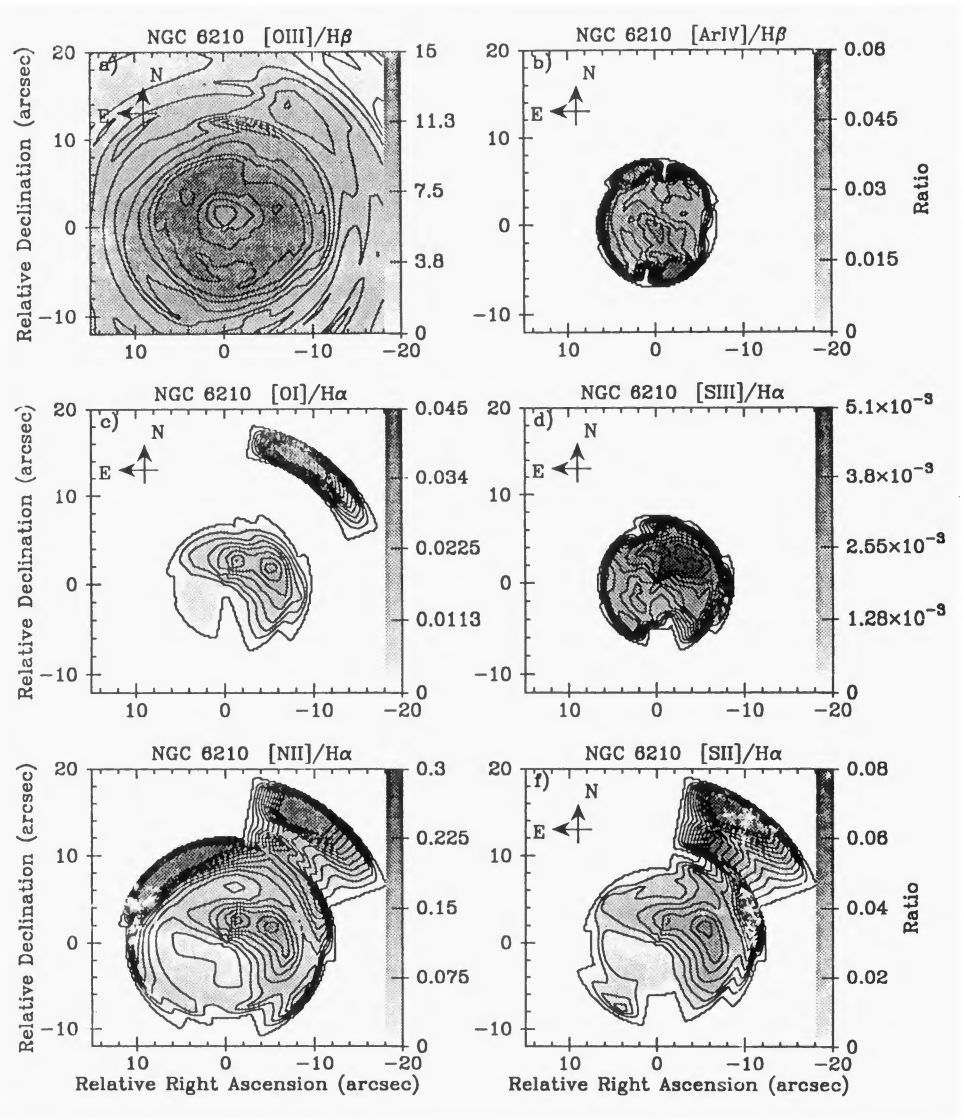

FIG. 3. Maps of line ratios over the core and halo of NGC 6210.

Finally, it is apparent from Fig. 8 that the location of the halo condensation is close to the maximum departure in line velocity. The effect of this is most vividly demonstrated if we compare Hα IDS emission profiles for P.A.'s 350° and 333°, in which the spectra have been integrated between radial displacements −18.5 and −15.5 arcsec, a 3 arcsec range which includes most of the emission in the condensation. The results, indicated in Fig. 12, are startlingly different given the relative proximity of the emission zones. The condensation (P.A.=333°) for instance is bodily shifted some ~35 km s^{-1} to longer wavelengths compared to the emission for P.A.=350°, while the width of this feature, against all expectations, is approximately 40% less.

3.4 Kinematics of the Core Zone

The core region again shows a distinct dichotomy in velocity structure, although of a rather different kind to that described for the halo. In particular, it is apparent that for position angles 330°–340° the positive and negative velocity components take the forms of arcs, centered upon the nucleus, and suggestive of expansion by a spheroidal shell (e.g., Fig. 7); although it may be noted that unlike the cases of regularly expanding shells such as NGC 7662 (e.g., Pottasch 1994), there is a distinct velocity discontinuity at maximum spatial displacements, close to the commencement of the halo. It is as though we were observing partial shells located on opposing sides of the central star.

For orthogonal position angles 30°<P.A.<80°, by contrast, the opposing shell components display highly tilted, linear, and broadly parallel velocity trends, with some curvature again occurring close to the commencement of the halo. Intermediate P.A.'s (110°–140°; 350°–0°) possess a mixture of both of these sets of properties.

As a result, maps of core Hα velocity appear highly tilted along a P.A.≅335° (Fig. 13), with both negative and positive components displaying similar trends; in consequence of which velocity difference maps appear to be comparatively invariant.

[N II] line velocities in large part mimic the Hα variation, although with one or two notable differences. In particular, it is apparent that [N II] expansion velocities are considerably

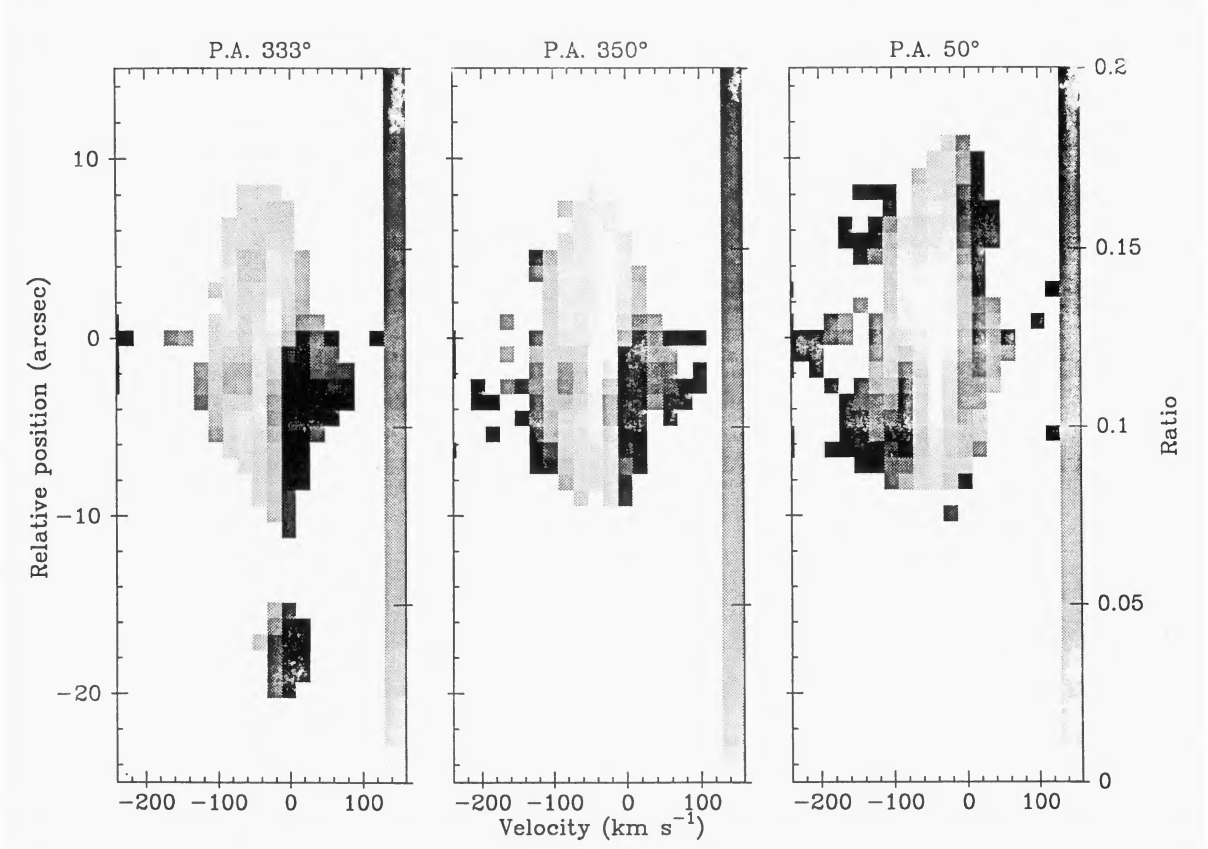

FIG. 4. Ratio between intermediate resolution [N II] λ6584 and Hα spectra for three position angles. It will be noted that a mix of high and low values of this parameter are to be found at most relative positions, suggesting appreciable line-of-sight variations in shell excitation.

greater than for Hα, a trend which, together with the comparatively low nuclear [N II]/Hα ratios, leads to the much more prominent line splitting noted in our IDS spectra (see Fig. 5). Secondly, it is apparent that [N II] emission is characterized by much larger fluctuations in intensity, arising perhaps from fragmentation of the [N II] emission zone. As a consequence, [N II] velocity determinations are available for only limited regimes of axial displacement.

3.5 Linewidths

Hα linewidths in the nucleus and halo appear to be both appreciable and highly variable. It is clear, for instance, that widths in the nucleus vary by up to ~15 km s^{-1} as between "front" and "rear" shells (hereafter assumed to refer to the negative and positive velocity components, respectively), while corresponding maps reveal a peculiar lopsided trend, with the front component favoring high values to the south and west, and the rear component to the north and east (Fig. 14).

For most of the P.A.'s investigated here, the Gaussian fitting routine resulted in satisfactory fits to the overall line shapes, and relatively low errors in estimated width. As in the case of the halo velocities noted in Sec. *3.3*, however, observations for a P.A. of 333° suggest a quite different story; Gaussian fits yield relatively large line width errors, suggesting the presence of significantly non-Gaussian line shapes. This trend is not shared by line profiles derived from closely adjacent emission zones (P.A.'s 330° and 335°).

Finally, halo linewidths appear to be characterized by an extremely unusual radial variation, involving first a rapid increase, then decrease, and then at large axial displacements a further possible increase and decrease in amplitude. The sizes of these variations are typically ~10–20 km s^{-1}, while the mean linewidth is of order ~50 km s^{-1}. The peak of the interior maximum occurs at somewhat different locations for the various P.A.'s, with clear evidence for a variation in antiphase with line centroid velocities where the latter vary most appreciably, that is, close to the halo condensation line P.A.=333° discussed above. Meanwhile, linewidth maps (Fig. 11) suggest a more-or-less consistent trend, in which large values of width occur for radii ~14 arcsec, and somewhat lesser values characterize the interior zones.

4. PHYSICAL CONDITIONS WITHIN NGC 6210

Using the low-resolution observations described in Sec. 3, we are able to determine the projected spatial variations in number of physical parameters relating to the shell and halo in NGC 6210. The various results are summarized below.

4.1 Extinction

The extinction c for this source has been variously estimated by Kaler (1986), Aller & Czyzak (1989), and Pottasch 1984), with resulting values ranging between 0 and 0.12. In the present case, we have used the Hα, Hβ, and Hγ transitions to evaluate extinction separately for all six of the low-

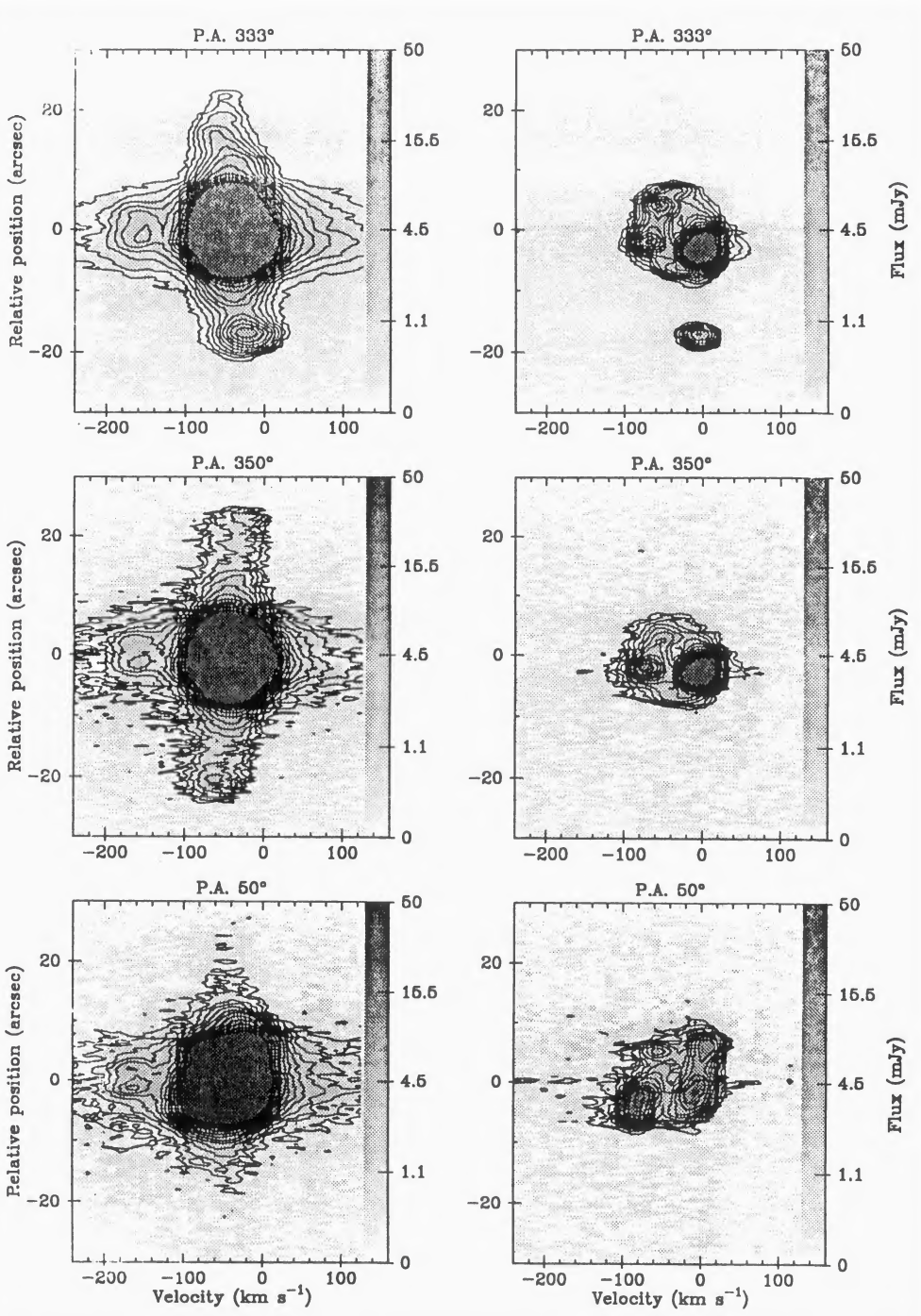

FIG. 5. IDS profiles for the Hα (left-hand panel) and [N II] λ6584 transitions along various P.A.'s. The faint spatial extensions to the Hα line arise from emission in the halo, while emission peaks close to λ=6560 Å derive from the He II 4^2F-6^2G transition. Note the strong condensation or "ansa" at P.A.=333°; a feature which is located exterior to the main shell, and is present in both Hα and [N II].

resolution spectra; where we assume case B conditions, adopt mean values of temperature and density similar to those to be described in the proceeding sections, and employ a reddening curve due to Whitford (1958). The corresponding mean estimate is found to be $c=0.047\pm0.019$. We see no significant evidence for spatial variations in extinction (although these are extremely difficult to assess given the low value of c); a result in general agreement with the polarization studies of Johnson & Jones (1991), where it is proposed that most if not all of this reddening is interstellar in origin

4.2 Temperature

Temperatures have been estimated for each spectrum using the usual ratio between [O III] λ4363, λ4959, and λ5007, together with an iteration procedure allied to the [S II] results described below. The resulting map is reproduced in Fig. 15, whence it is apparent that T_e peaks at $\sim 1.1\times10^4$ K close to the center, and thereafter declines more-or-less symmetrically towards the periphery by a factor ~0.25. Note, how-

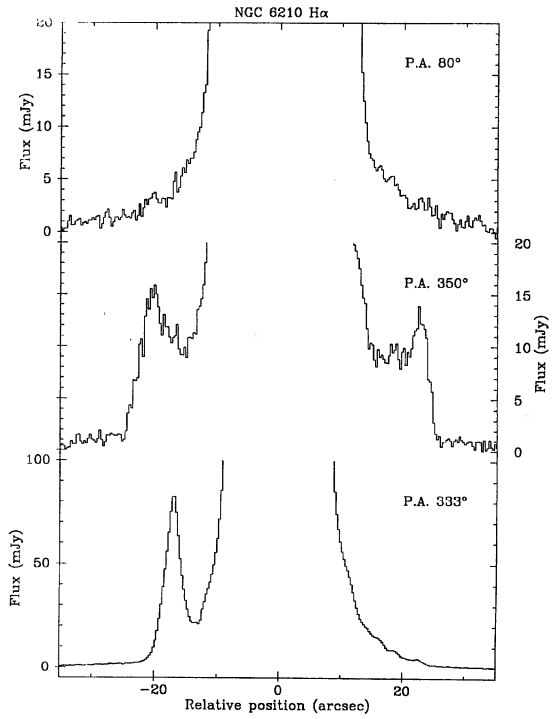

FIG. 6. Hα emission profiles through the nucleus of NGC 6210, where we have expanded the intensity scale to reveal details of the halo structure. Notice in particular the strong secondary emission peak along P.A.=333°, close to RP=−17 arcsec.

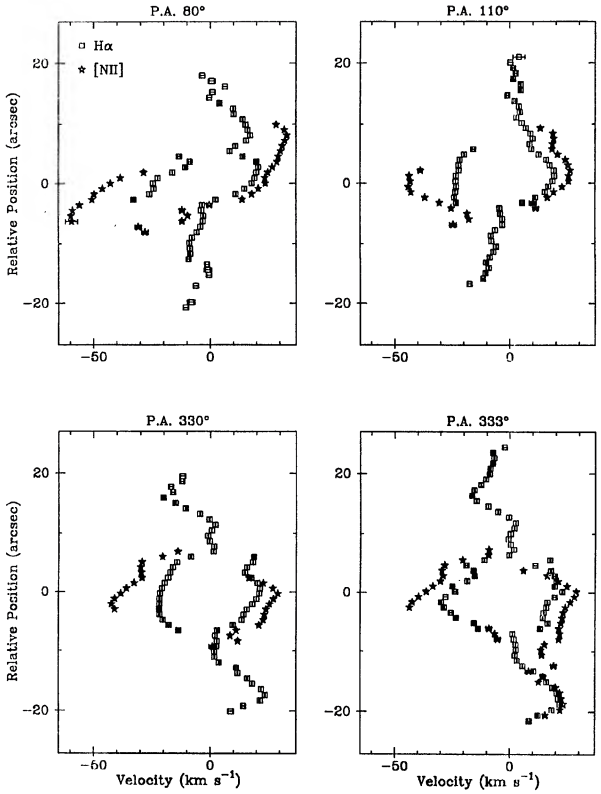

FIG. 7. Variation of Hα and [N II] λ6584 line centroid velocities through the nucleus of NGC 6210, where we illustrate the trends for four characteristic P.A. The lines divide into two components within the nucleus, corresponding to front and rear shells, but appear otherwise to arise from a single kinematic component.

ever, the slight leaning towards higher temperatures in the north, and some further increase in temperatures towards the outer parts of the shell.

Intensities for the λ4363 line at locations close to the ansa are insufficiently high to determine an accurate temperature, although for the intensity limits summarized in Table 1 it is clear that $T_e<11\,560$ K.

4.3 Density

Densities in NGC 6210 have been assessed in a similar manner to that described for temperatures in Sec. *4.2*, using in this case the λλ 6717+6731 Å transitions of [S II]. The resulting map appears to be significantly lop-sided (Fig. 16), with values appearing particularly high to the north of the central star, where they achieve a maximum $n_e=6.1\times10^3$ cm^{-3}. Interestingly, a comparison of this map with the radio observations of Terzian (1987) suggests broadly similar structures, implying that much of the variation in radio emission may arise from corresponding variations in density.

Given that temperatures are not available for the exterior condensation (see Sec. *4.2*), it follows that densities must remain somewhat speculative. Assuming however a mean temperature of 10^4 K (and the density is in any case not sensitively dependent upon this parameter), we find a peak in density at the condensation of 1.8×10^3 cm^{-3}, falling symmetrically to $\sim9.9\times10^2$ cm^{-3} at locations 0.9 arcsec either side of the core. A mean based upon line intensities provided in Table 1 (i.e., for emission integrated over a 1×3 arcsec^2 slice through the ansa) suggests $\langle n_e\rangle=1.24\times10^3$ cm^{-3}.

5. SPATIO–KINEMATIC STRUCTURE OF NGC 6210

5.1 Properties of the Halo Condensation

From the summary of observations provided in Sec. 3, it is clear that the condensation constitutes a particularly bright component within a dual jet-like formation. Temperatures appear not to exceed those expected of a photoionized region, and any excitation by shocks would be required to be to be comparatively weak. Similarly, densities are reasonably modest, and comparable to those in the central nebula. Taking a deconvolved FWHM of order $\theta_w=2.75$ arcsec, and estimating the flux within a circle of this size to be $\sim1.9\times10^{13}$ ergs cm^{-2} s^{-1} (Fig. 6; we have approximately corrected for more generalized halo emission, and assumed circular symmetry), we can then derive a depth for the region $\cong0.036$ pc, corresponding to an angular size $\theta_d\cong5.7$ arcsec, where we have assumed a temperature $T_e=10^4$ K, distance $D=1.3$ kpc (Sabbadin & Hamzaoglu 1982), and adopted case B conditions. The closeness of θ_d to θ_w suggests that given the overall uncertainties and simplifications, the deduced physical characteristics cannot be too greatly in error.

Similarly, for an entity which is completely ionized, the expansion timescale would be on the order of $\tau_{\rm exp}\sim4.75\times10^3$ ($^a\theta_w$/arcsec)(D/kpc/(2V_a/km s^{-1}))yr$\sim$425 yr; a value which is significantly less than the probable age of the nebula. It follows that where the ansa condensation is

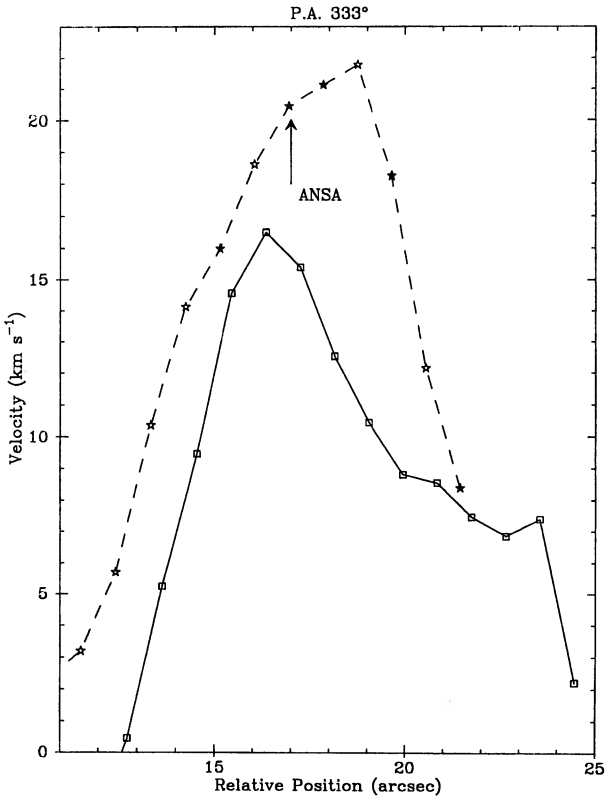

FIG. 8. Variation in the modulus of jet radial velocity along P.A.=333°, where we have superimposed trends for the positive (- - - - - - - -) and negative (----------) axial displacements (i.e., respectively for the SE and NW jet extensions). Note that in reality, radial velocities to the SE are negative compared to the nebular mean velocity, and those to the NW are positive. The nebular condensation/ansa appears to be located close to the position of peak velocity in the northwesterly jet.

directly expelled from the central star, then radial velocities would be required to be in excess of 250 $(\sin i_a)^{-1}$ km s^{-1}, where i_a is the inclination between the velocity vector and the plane of the sky.

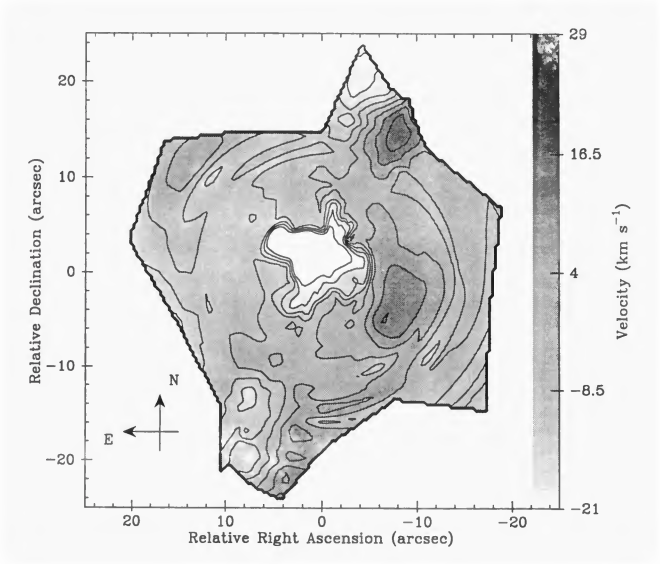

FIG. 9. Variation of projected Hα velocities for the NGC 6210 halo, where it may be noted that the jet-like feature causes a distinct warping of contours about a P.A.=333° (i.e., along the NW-SE map extension).

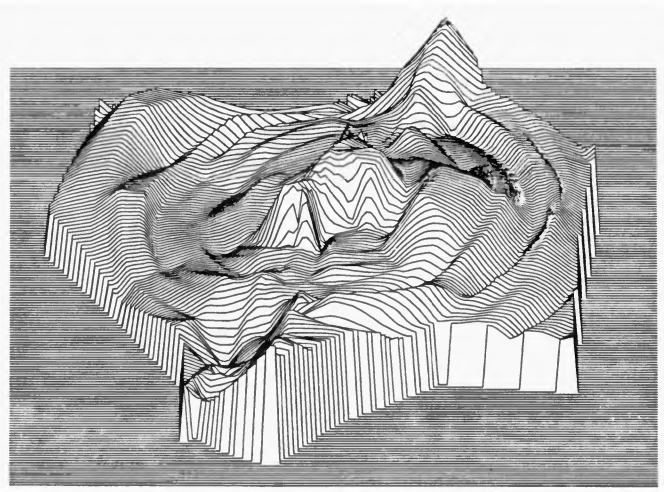

FIG. 10. A relief map of the halo velocity field, showing more clearly the presence of circularly symmetric ripples, and a strong bipolar flow to the NW and SE.

High levels of low-excitation emission may derive from strong local stratification, of type previously discussed by Capriotti (1973), as well as through UV shadowing effects similar to those used to explain the small-scale structures in NGC 7293, and high levels of low-excitation emission in certain bipolar nebulae (Cohen 1983). Local shocks may also play a role in preferentially exciting certain low-excitation species, including both [S II] and [N II].

Finally, we note that such features may also arise as a direct consequence of shock interaction between the jet and envelope, as discussed by Soker (1990). For this case, the persistence of such features depends primarily upon the lifetime of the jet, and the continuance or otherwise of current mass-flow rates and velocities.

5.2 Structure of the Core

The kinematic observations of the core discussed in Sec. *3.4* are, we believe, open to a relatively simple (if somewhat

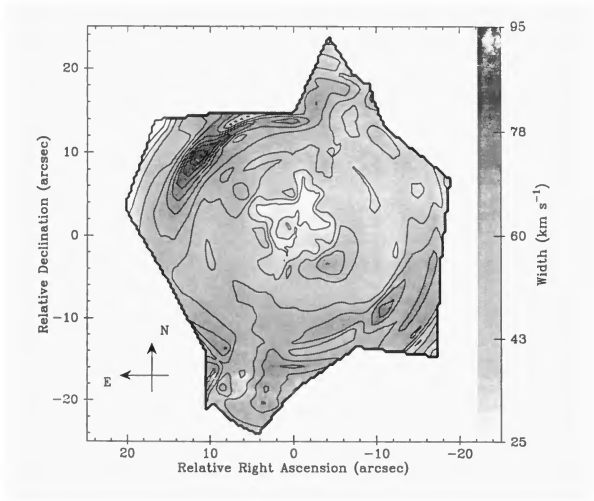

FIG. 11. Variation of Hα linewidths within the halo. In this case, the jet appears to be characterized by reduced linewidths, whilst a ring of enhanced velocities encircles the inner halo at distance ~14 arcsec from the nucleus. The inner core is represented by the rear shell; separate maps of this regime are illustrated in Fig. 14.

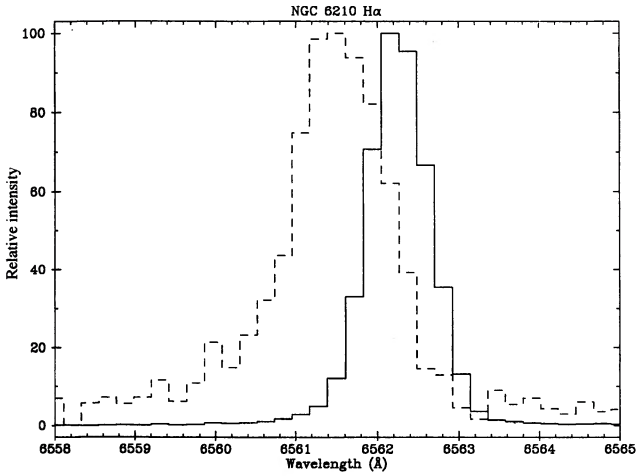

FIG. 12. Hα line profiles for position angles 350° (dashed curve) and 333° (solid curve), integrated between relative positions −18.5 and −15.5 arcsec. The profile at 333°, corresponding to the bright halo condensation, is both shifted and narrower compared to the closely adjacent emission regime.

unusual) explanation; the tendency for shell-like expansion throughout the range of P.A.'s 330°–340°, and tilted, parallel velocity trends along orthogonal directions, would argue for a cylindrical structure tilted to the line of sight. Given this type of model, the observations can probably then best be explained if we presume a high level of ionization stratification (i.e., that the [N II] lines arise primarily in the outer part of the shell), a substantial radial velocity gradient [yielding greater line splitting for the [N II] transitions, as compared to Hα (see Fig. 7)], and some fragmentation of the shell at larger radii (giving rise to the more fragmentary [N II], structure, again compared to Hα). The velocity "curvature" at the limits of the interior nebula, evident where the trends are predominantly parallel, presumably arise at the limits of the cylindrical shell. These peculiarities, in turn, are probably best explained in terms of local deformation of the shell, arising from shock interaction with interior winds, or as a consequence of partial closure of the shell in a manner similar to that envisaged for NGC 6905 (Cuesta *et al.* 1993), where it has been proposed that interior winds may be responsible for punching symmetrically located holes within the primary outflow shell. Under these circumstances, the disparity between the projected curvatures of front and rear shells can be shown to imply an angle of inclination $i=67°$.

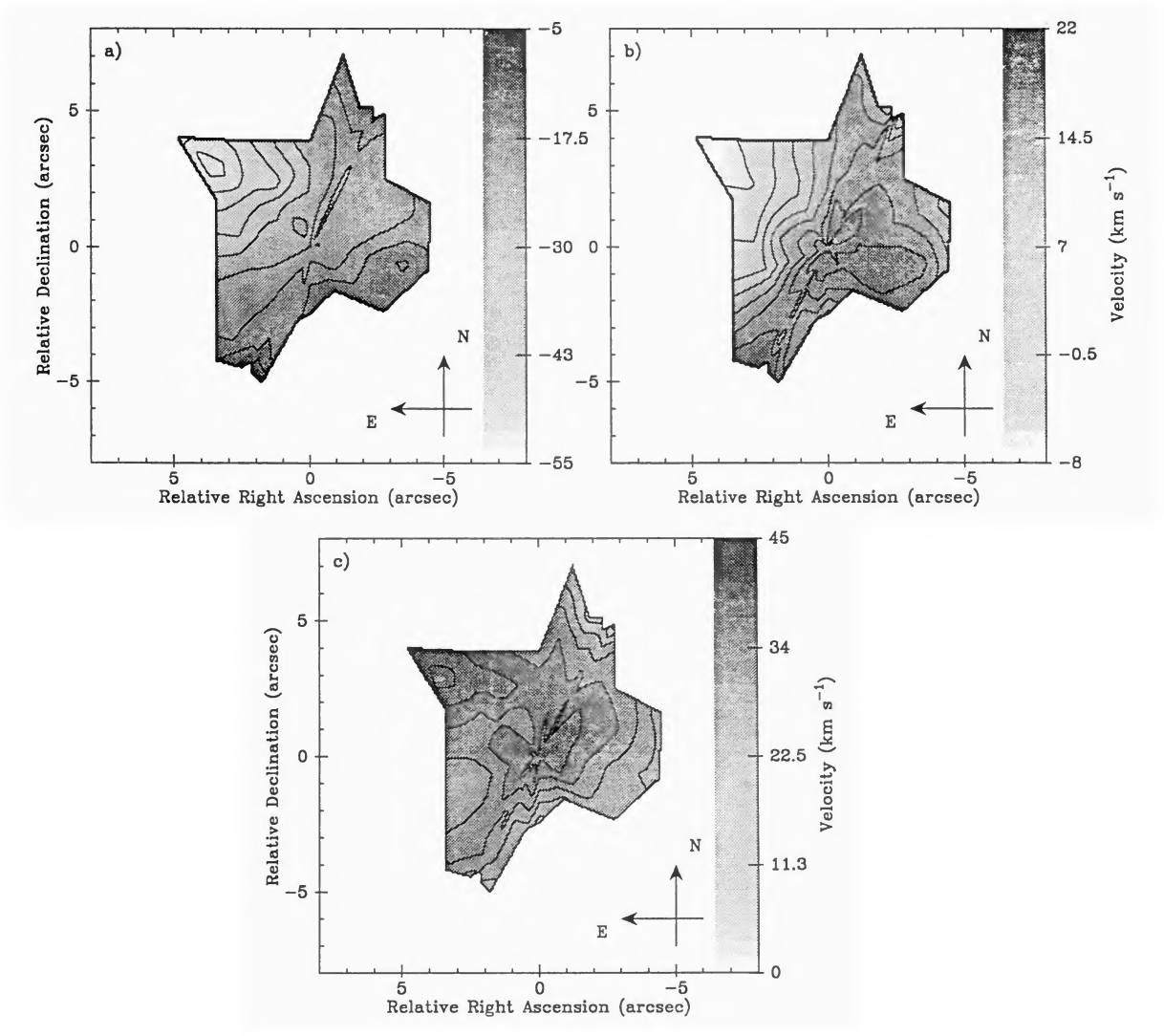

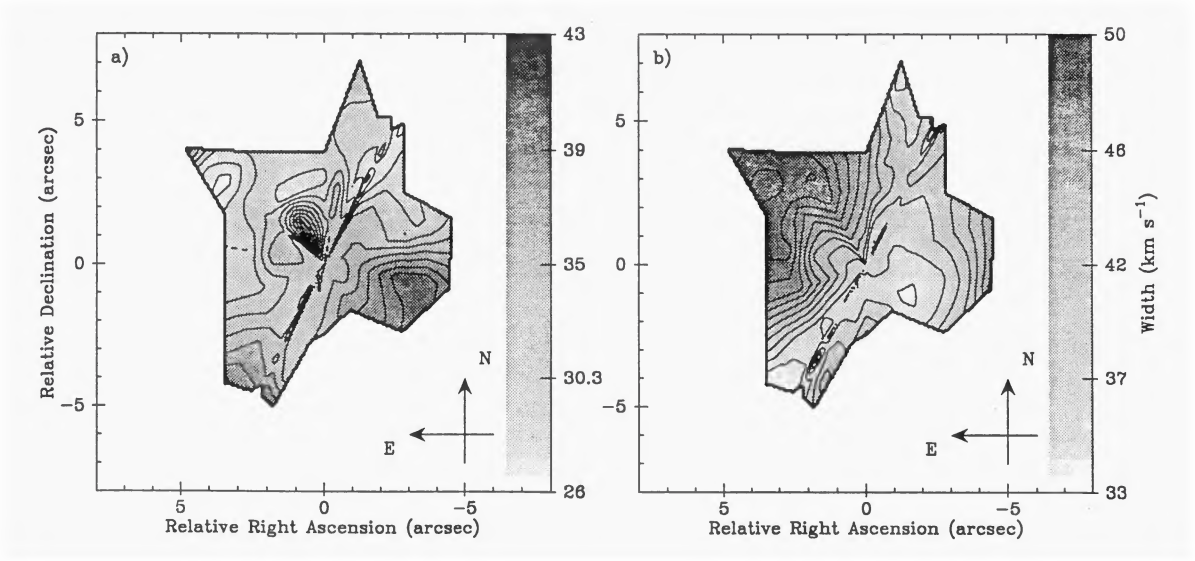

FIG. 14. Variation in Hα linewidths over the core of NGC 6210, where it is clear that the spatio-kinematic distributions of front and rear shells differ markedly. There is again, however, a clear indication of kinematically quite distinct properties as between eastern and western sectors of the shell.

This model is, however, almost certainly too simplistic. A radial velocity field, for instance, together with corresponding variations in density, would normally be expected to lead to reduced linewidths at large axial displacements from the nucleus. The reverse is observed (cf. Fig. 14). Such a result might well imply appreciable nonsymmetric variations in shell density, a feature for which we already have clear evidence from our mapping (see Fig. 15). In addition, it is apparent that orthogonal spectral cuts to the presumed cylinder axis do not produce the simple bow-shaped line profiles characteristic of spheroidal shells, but rather, imply two arcs separated by a velocity discontinuity (Sec. *3.4*).

Tying these various features together, we believe that any model capable of unifying these disparate characteristics must have at least some of the properties illustrated in Fig. 17. We have few illusions concerning the finality of this model, however, and can only affirm that whatever structure the core should finally prove to possess, it will differ significantly from the simple morphologies which appear to characterize many other PN.

5.3 Characteristics of the Jet and Halo

The overall image of the halo which appears to emerge from these observations is of a circularly symmetric structure with low excitation, disturbed by low amplitude velocity waves, and containing four symmetrically opposed, appreciably curved emission arms. At least one, and possibly both sets of arms are associated with substantial kinematic irregularities; a characteristic which appears to be particularly enhanced within $\sim\pm2.5°$ of P.A.$=333°$, to extend throughout the primary halo region, and to influence line profiles in the interior shell.

These trends are also associated with corresponding enhancements of low-excitation emission.

Whatever the origin of these properties, we are clearly dealing with a comparatively tightly focused kinematic event; a feature which is likely to have arisen from a phase of collimated ejection near the central star. The present axis of ejection is close to P.A. $\sim333°$, although curvature of the emission arms at larger radial distances may testify to a

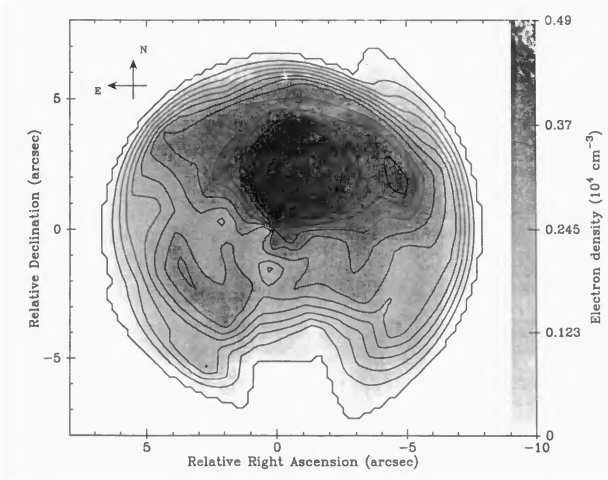

FIG. 15. Variation of electron density over the primary envelope in NGC 6210 (see text for details).

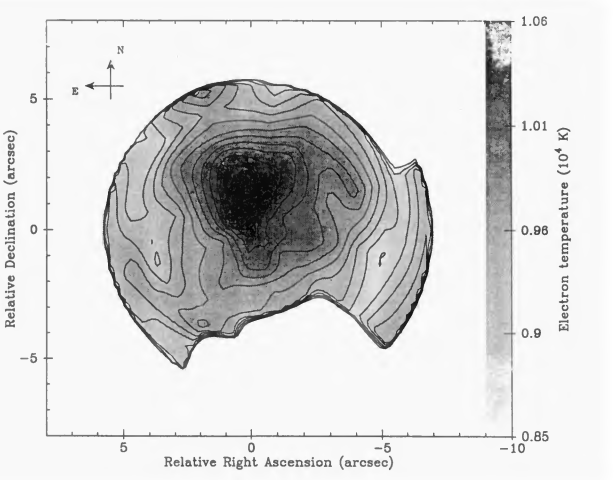

FIG. 16. Variation of electron temperature over the primary envelope in NGC 6210 (see text for details).

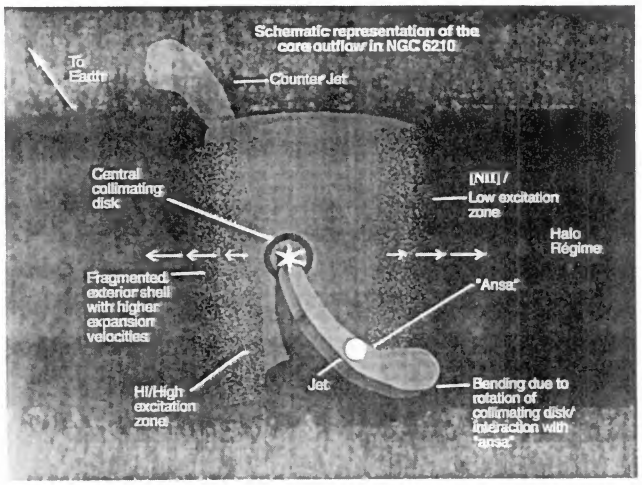

FIG. 17. Model for the central envelope in NGC 6210, in which we suppose that the primary shell may be described in terms of a tilted pseudocylindrical configuration.

slightly differing angle of ejection in the past, implying perhaps that the orientation of the collimating zone is also slowly changing (see the discussion in Sec. 6). The bright halo condensation may result from an unusually intense phase of mass ejection, or interaction of the jet with mass condensations in the exterior envelope.

One further consequence of such model would be for increasing diffusion of the jet as distance from the nucleus increased, supposing always that the width of spectral lines along the jet outflow axis implies a species of expansion, and that lateral confinement of this motion is not unduly severe. Such behavior appears to be qualitatively supported by our observations. Given an intrinsic jet outflow velocity V_J, therefore, and transverse expansion velocity ${}^{J}V_{\rm exp}\sim 40$ km s^{-1} (e.g., Fig. 12), the projected jet aspect ratio $\Lambda_J>3$ would imply $V_J>120\,\sin(i_j)^{-1}$ km s^{-1}.

• It remains unclear whether the separate (weaker) arms of emission extending along P.A. $\sim 105°$ represent a current phase of mass expulsion, or an enhancement associated with an earlier period of mass loss. Perhaps mass expulsion occurs in relatively distinct phases as the collimating regime rotates, and the weaker arms represent a fossil remnant of this prior activity? Similarly, if the mass expulsion events have extended over an appreciable length of time, there exists the possibility that they are directly feeding the exterior halo mass, and may be responsible for much of the observed extended emission.

The variation in line centroid velocities and absence of kinematic stratification (e.g., larger linewidths for [N II] compared to H I, or related line splitting) may indicate the presence of a highly fragmented, spatially unresolved shell structure, although the large linewidths noted in Sec. *3.5* would in that case be less easy to comprehend. One mechanism for generating such features might be for shock heating of the exterior shell, related perhaps to the ripples observed within the halo velocity field. A problem with this hypothesis, however, is that linewidths of heavier ionic species such as N^+ would be expected to be appreciably reduced compared to the Balmer lines; a prediction which appears not to be consistent with our present results. Similarly, for a shock propagating through ionized gas with velocity V_s, the immediate post-shock temperature would be $T_s=3\mu_s m_H V_s^2/16k\approx 14.4\,(V_s/\text{km s}^{-1})^2$, where μ_s (=0.636) is the mean atomic weight per particle, and following Shull & Draine (1987) we assume H and He to be singly ionized, and to have a number density ratio He/H=0.1. If observed linewidths W arise primarily through thermal excitation, therefore, it follows that $V_s\cong\mu_s^{-0.5}W\cong 65$ km s^{-1}, and immediate post-shock temperatures would be of order $T_s\sim 6\times 10^4$ K.

For shocks having these or similar velocities, the variation of temperatures in the post-shock cooling zone has been analyzed by Seab & Shull (1985). As a consequence, it is apparent that for a strong adiabatic shock, enhanced post-shock excitation would be largely dissipated within a distance $d_s\sim 3\times 10^{17}\,(n_0/\text{cm}^{-3})$ cm of the front, where n_0 is the pre-shock density; that is, within a projected angular range $\theta_s\leqslant 5/[(n_0/\text{cm}^{-3})(D/\text{kpc})]=0.04$ arcsec. Such enhanced regions of heating are therefore extremely narrow, and would be incapable of maintaining the observed broad emission linewidths except by a process of continuous and frequent shocking.

In brief, the unusual pattern of halo kinematics remains far from easy to understand, and deeper spectroscopy would be of considerable help in constraining the mechanisms described above.

6. DISCUSSION

The relatively high level of collimation in the jet places it among a select group of nebulae, in which these or similar features appear to constitute separate kinematic entities within the primary outflow structure. Low collimation flows in (mainly) type I nebulae have been investigated intensively in recent years (see, for instance, Phillips 1989 and Corradi & Schwarz 1995), and seem likely to arise as a consequence of the direct collimation of stellar winds by a circumstellar disk. The precise origin of this collar or disk is a matter of continuing debate, with possible contributions arising from a mix of stellar rotation, magnetic fields, protostellar material, and so forth (cf. Field & Abbott 1986; Poe & Friend 1986; Pringle 1989; Pascoli 1987). Perhaps the most popular model, however, certainly the most proselytized, supposes an initial transfer of mass between the primary and secondary components of a close binary system, as discussed by Bond & Livio (1990).

It remains far from clear, however, how such a mechanism would account for the exceptionally high level of collimation evident in the present source, or indeed, for the similar features noted in *K* 1–2 (Bond & Livio 1990), NGC 3242 (Soker 1992), NGC 2392 (Gieseking *et al.* 1985), and NGC 7009 (e.g., Balick 1987). In the first place, it is clear that many if not all of these jets derive from a locale close to the central star, and are at least partially located within already well evolved shells; a trend which presumably implies a more recent provenance for the collimating regime than is the case for the exterior envelope. Secondly, there is the problem of how to develop and maintain the observed large aspect ratios. Although Icke *et al.* (1992) have developed

models in which inertial collimation and oblique interior shocks result in jet-like structures, Soker & Livio (1994) have noted that these or similar flows demand a series of comparatively unrealistic conditions, including high density contrasts, and a method of feeding pressure within the confining material. In general, it seems likely that the formation of such jets depends upon two primary requirements: an accretion disk, and the presence of magnetic fields in order to both accelerate and confine the flow (Blandford 1993; Pringle 1993; and Soker & Livio 1994).

It is probable, therefore, that such nebulae are displaying a series of comparatively late evolutionary changes, associated with subsequent evolution of the central binary system; a stage in which a secondary phase of mass transfer and expulsion is occurring, associated with extraordinarily high levels of flow confinement. Alternatively, it may be possible that backflow of the evolved shell is responsible for the setting up of an accretion disk about the central star, as recently investigated by Soker & Livio (1994), a development which may occur during relatively late stages in the evolution of the primary shell. In either case, the combined evidence of possible jet rotation, large aspect ratios, velocity vectors, and emission structures favors a flow inception and collimation regime extremely close to the core binary system.

Finally, we note that bending of the jet may, as surmised earlier, arise from temporal reorientation of the collimating zone; perhaps as a consequence of precession within a binary system. Alternatively, Soker (1990) has noted a similar tendency for reorientation of jets beyond the bright ansae in NGC 3242 and NGC 7009; a trend which is attributed to the influence of (oblique) shock interaction between the primary shell and interior jet flow. The apparent presence of similar spatio-kinematic trends in all three sources is certainly interesting, and suggests an underlying commonality of both outflow properties and driving mechanisms. This may also extend to the extremely diffuse source DS1, which is centered upon an eclipsing binary KU Vel having period 0.357 days (Bond & Livio 1990). In this case, there appears to be no evidence for a jet in [O III] images of the source, although the shell is possessed of four curved arm-like features, disposed in pairs upon opposing sides of the nucleus. The broad similarity to the NGC 6210 halo structure is certainly striking; although the greater widths, and lesser arm/halo emission contrast may testify to a later phase of evolution.

To conclude, therefore, it is apparent that this superficially unprepossessing source is characterized by an exceptionally unusual suite of properties, the implications of which remain deeply ambiguous. Further observations will certainly be required in order to clarify the source structure and kinematics, and, most importantly, to identify the mechanisms responsible for such anomalous behavior.

7. CONCLUSIONS

We have observed the extended post-main-sequence source NGC 6210 along 11 position angles through the nucleus. The resulting low- and intermediate-resolution spectroscopy has subsequently been used to evaluate the two-dimensional variations in a broad range of parameters, including temperature, density, line excitation, linewidth, and velocity.

The temperature variation is perhaps the least complex of this data set, revealing peak values $T_e \sim 1.10 \times 10^4$ K close to the nucleus, declining to $T_e \sim 8.3 \times 10^3$ K over projected distances of ~8 arcsec. Density variations are marked by a greater degree of variability, and imply preferentially elevated values $n_e \cong 6.1 \times 10^3$ cm^{-3} towards the north, and somewhat more depressed values $n_e \sim 1.5 \times 10^3$ cm^{-3} to the south; a trend which is reminiscent of, and presumably directly responsible for observed variations in radio continuum emission.

This relative complexity of structure is even more apparent in maps of line excitation, where it is clear that low-excitation lines are enhanced to the north and west, and along extensions having P.A.=333°. These nebular "arms," evident in direct photographs of the halo, appear to extend on either side of the core, and are associated with an intense condensation having peak density $n_e \cong 1.8 \times 10^3$ cm^{-3}. A secondary set of arms along P.A. ~105° appear morphologically similar (if somewhat weaker), and have presumably also been generated in a similar manner, although the kinematic and excitation structures are less distinctive.

The low-excitation halo extensions are also associated with a narrowly focused kinematic disturbance, resulting in line-of-sight velocity variations of order $\Delta V \cong 30$ km s^{-1} within the halo, and appreciably deformed line profiles within the primary shell (a consequence either of line blending and/or direct interaction). We propose that this suite of properties indicates (possibly continuous) shock interaction between the ionized shell and a high velocity jet. This jet shows evidence for increasing diffusion at larger radial distances, and appreciable curvature, a trend which may derive from rotation of the collimation zone as a consequence of precession within a binary system, or through oblique shock interaction between the jet and halo. Continuous activity of this nature may also be responsible for generation of the halo, with source DS1 representing a more advanced phase of this process.

Although the broad linewidths and large densities observed along the NW jet axis may conceivably derive from shock activity, this constitutes a less plausible mechanism for the halo as a whole, where linewidths approach $\Delta W \cong 50$ km s^{-1}; we suggest that post-shock heating of the halo would require an excessive level of shock excitation.

It seems likely nevertheless that low amplitude, more-or-less circularly symmetric ripples occur within the velocity field of the exterior shell, and may be responsible for more limited excitation at particular halo locations.

The core Hα velocities show a distinct E-W dichotomy, with high positive velocities to the west, and corresponding negative velocities to the east. These, together with the corresponding N-S trend in Hα line velocity, and more fragmentary data for [N II], are far from easy to comprehend. It seems likely, however, that we are observing a distorted cylindrical structure tilted to the line of sight, perhaps the disrupted remnant of an initially spheroidal shell. If this is the case, then we have a somewhat perplexing situation whereby

collimated mass loss is oriented perpendicular to the principal axis of the cylinder.

Clearly, the present observations have provoked at least as many questions as they have resolved. The only characteristic that is unambiguously clear is that we have, in this source, an exceptionally interesting and complex suite of phenomena characteristics which deserve considerably more investigation than has been the case heretofore.

We would like to thank staff at the Observatorio de los Muchachos for their assistance during the taking of these observations, and an (anonymous) referee for drawing our attention to an early image of this source by Duncan (1937). The 2.5 m INT is operated on the island of La Palma by the Royal Greenwich Observatory in the Spanish Observatorio del Roque de los Muchachos of the Instituto de Astrofisica de Canarias.

REFERENCES

Aller, L. H., & Czyzak, S. J. 1983, ApJS, 51, 211
Aller L. H., & Epps, H. 1975, ApJ, 204, 445
Balick, B., Gonzalez, G., Frank, A., & Jacoby, G. 1992, ApJ, 392, 582
Blandford, R. 1993, in Astrophysical Jets, edited by D. Burgarella, M. Livio, and C. O'Dea (Cambridge University Press, Cambridge), p. 15
Bond, H. E., & Livio, M. 1990, ApJ, 355, 568
Capriotti, E. R. 1973, ApJ, 179, 495
Cerruti-Sola, M., & Perinotto, M. 1989, ApJ, 345, 339
Cohen, M. 1983, in Planetary Nebulae, IAU Symposium No. 103, edited by D. R. Flower (Reidel, Dordrecht, Holland), p. 45
Corradi, R. L. M., & Schwartz, H. E. 1995, A&A, 293, 871
Cuesta, L., Phillips, J. P., & Mampaso, A. 1993, A&A, 267, 199
Duncan, J. C. 1937, ApJ, 86, 496
Friend, D. B., & Abbott, D. C. 1986, ApJ, 311, 701
Gieseking, F., Becker, I., & Solf, J. 1985, ApJ, 295, L17
Icke, V., Mellema, G., Balick, B., Eulderink, F., & Frank, A. 1992, Nature, 355, 524
Icke, V., Preston, H. L., & Balick, B. 1989, AJ, 97, 462
Johnson, J. J., & Jones, T. J. 1991, AJ, 101, 1735
Kaler, J. B. 1986, ApJ, 308, 322
Pascoli, G. 1987, A&A, 180, 191
Perinotto, M. 1993, in Planetary Nebulae, IAU Symposium No. 155, edited by R. Weinberger and A. Acker (Kluwer Academic Publishers, Dordrecht, Holland), p. 57
Phillips, J. P. 1989, in Proceedings of the XIth Regional Astronomy Meeting of the IAU, edited by F. Sanchez and M. Vazquez (Cambridge University Press, Cambridge)
Poe, C. H., & Friend, D. B. 1986, ApJ, 311, 317
Pottasch, S.R. 1994, Planetary Nebulae (Reidel, Dordrecht)
Preite-Martinez, A. 1993, in Planetary Nebulae, IAU Symposium No. 155, edited by R. Weinberger and A. Acker (Kluwer Academic Publishers, Dordrecht, Holland), p. 65
Pringle, J. E. 1989, in Theory of Accretion Disks, edited by F. Meyer *et al.* (Kluwer Academic Publishers, Dordrecht, Holland)
Pringle, J.E. 1993, in Astrophysical Jets, edited by D. Burgarella, M. Livio, and C. O'Dea (Cambridge University Press, Cambridge), p. 1
Sabbadin, F., & Hamzaoglu, E. 1982, A&A, 110, 105
Seab, C. G., & Shull, J. M. 1985, Interelationships among Circumstellar, Interstellar, and Interplanetary Grains, NASA CP-2403, p. A-28
Shull, J. M., & Draine, B. T. 1987, in Interstellar Processes, edited by D. J. Hollenbach and H. A. Thronson, Jr. (Reidel, Dordrecht, Holland), p. 283
Soker, N. 1990, AJ, 99, 1869
Soker, N. 1992, ApJ, 389, 628
Soker, N., & Livio, M. 1994, ApJ, 421, 219
Balick, B. 1992, AJ, 104, 2151
Stanghellini, L., & Kaler, J. B. 1989, ApJ, 343, 811
Terzian, Y. 1987, S&T, February, p. 459
Whitford, A. E. 1958, AJ, 63, 201